Electronic Supplementary Information (ESI) for

Engineering bimetal Cu, Co sites on 3D N-doped porous carbon nanosheets for enhanced oxygen reduction electrocatalysis

Linzhi Lu, [‡a] Ying Liu, [‡a] Jiayao Fan,[a] Lei Wang,[a] Yue Lin,*[b] Dongdong Xu,[a] Zhihui Dai,[a] and Min Han*[ac]

[a] Jiangsu Key Laboratory of New Power Batteries, and Jiangsu Key Laboratory of Biofunctional Materials, School of Chemistry and Materials Science, Nanjing Normal University, Nanjing 210023, P. R. China.

E-mail: 07203@njnu.edu.cn

[b] Hefei National Laboratory for Physical Sciences at the Microscale, University of Science & Technology of China, Hefei 230026, P. R. China.

E-mail: linyue@ustc.edu.cn

[c] State Key Laboratory of Coordination Chemistry, Nanjing National Laboratory of Solid State Microstructures, Nanjing University, Nanjing 210093, P. R. China

‡ L. Lu and Y. Liu contributed equally

Experimental Sections

Materials and Reagents: All the chemical reagents were obtained from available commercial sources without further purification. The $C_{12}H_{25}SO_3Na$ (SDS), $K_2S_2O_8$ (≥ 99.5%), melamine (≥ 99.0%) and styrene (≥ 99.0%) were obtained from Alfa Aesar. And the H_2SO_4 (95.0%~98.0%), $CoCl_2 \cdot 6H_2O$ (≥99.0%), and $CuCl_2 \cdot 2H_2O$ (≥99.0%) were obtained from the Sinopharm Chemical Reagent Co. Ltd. (Shanghai).

Synthesis of polystyrene (PS) spheres: In a typical synthesis, SDS (151.2 mg) and $K_2S_2O_8$ (200.0 mg) were firstly dissolved in a mixture of deionized water (117 mL) and ethanol (23 mL) under stirring in N_2-saturated atmosphere. After maintained at 70 ºC for 30 min, 7 mL of styrene (dispersed in 2M NaOH) were added dropwise. The obtained solution was kept stirring for another 6 h. Finally, the product was separated by centrifugation, and washed with water and ethanol for several times to remove the by-products. After freeze-drying for 4h, the PS spheres were obtained, and employed for the subsequent sulfonation reaction.

Synthesis of sulfoacid-functionalized polystyrene (SPS) spheres: The pre-synthesized PS spheres (1000 mg) were firstly dispersed in 15 mL of deionized water by ultrasonication for 10 min. Whereafter, 50 mL of concentrated H_2SO_4 were dropwise added into reaction system with continuously stirring to trigger the sulfonation reaction. After reacted for 24 h, the product was centrifuged and washed with deionized water for several times until the pH close to neutral. Finally, the SPS powder was obtained by freeze-drying overnight.

Synthesis of Cu,Co-N-C NSs: In a typical procedure, the pre-synthesized SPS spheres (0.3 g) were dispersed in 150 mL of deionized water under mechanical stirring to form a uniform suspension. Then, the $CuCl_2 \cdot 2H_2O$ (0.75 g), $CoCl_2 \cdot 6H_2O$ (1.05 g) and melamine (5.40 g) were added into the above suspension in turn. After continuously stirring at room temperature for 4 h, the desired precursors were obtained by centrifugation and then subjected to freeze-drying for 5 h. Subsequently, the obtained precursors were loaded into a clean ceramic boat, and placed in the central region of a horizontal tube furnace. By introducing Ar gas to expel the air for 30 min, the furnace was heated from room

temperature to 900 °C with a heating rate of 5 °C min^{-1}, and maintained at 900 °C for 1 h. After naturally cooled down to room temperature, the black crude product was obtained, which was further soaked in 0.5 M H_2SO_4 for 10 h and then re-annealed under Ar atmosphere at 900 °C for another 1 h to obtain the desired Cu,Co-N-C NSs.

Synthesis of Cu-N-C and Co-N-C counterparts: The synthetic process of Cu-N-C and Co-N-C counterparts were similar to that for Cu,Co-N-C NSs. The only difference lies on the used precursors that without adding $CoCl_2 \cdot 6H_2O$ and $CuCl_2 \cdot 2H_2O$, respectively.

Materials characterization: The field-emission scanning electron microscopy (FE-SEM) images were acquired on a JSM-7600F apparatus. And the transmission electron microscopy (TEM) and high angle annular dark field-scanning transmission electron microscopy (HAADF-STEM) images as well as elemental mapping patterns were obtained on JEOL-2100F and probe aberration-corrected JEM ARM 200F apparatuses, respectively. The XRD patterns were collected on a D/max 2500 VL/PC diffractometer (Japan) that equipped with graphite monochromatized Cu Kα radiation (λ = 1.54060 Å). And the induction coupled plasma atomic emission spectra tests (ICP) were executed on a Jarrel-Ash 1100+2000 Quantometer. The Raman spectra were recorded on a JY HR 800 (France) instrument with an optical multichannel spectrometer Microdil 28 (Dilor) equipped with a microscope. An objective with 100× magnification was employed both for focusing the excitation light (Ar^+ laser, 488 nm) and for collecting the scattered light. The N_2 sorption tests were performed on a Quantachrome Instruments Autosorb AS-6B. The Fourier-transformed infrared (FT-IR) spectra were obtained on a Vertex-70 spectrometer (Bruker). And the X-ray photoelectron spectroscopy (XPS) tests were carried out on a scanning X-ray microprobe (PHI 5000 Versa, ULACPHI, Inc.) with Al Kα radiation. As for electrochemical impedance spectroscopy (EIS) tests, they were performed on a CHI 660E electrochemical workstation under the actual ORR conditions at 298 K. The applied potentials were fixed at -0.15 V (*vs*. Ag/AgCl). All the EIS data were recorded at the frequency of 10^{-1}-10^6 Hz.

Electrocatalytic measurements: The electrocatalytic experiments were carried out on a Garmy's rotating ring-disk electrode (RRDE) that equipped with a CHI 700e electrochemical workstation. The diameter of the glassy-carbon disk in RRDE is approximately 5 mm. A standard three-electrode system

was adopted for all the tests. The Cu,Co-N-C NSs or other control catalysts modified RRDE were served as the working electrodes, and the Ag/AgCl and high-purity graphite rod or Pt foil were used as the reference electrode and counter electrode, respectively. For each test, the total loading amount of catalyst was fixed to be 0.204 mg cm^{-2}. The electrocatalytic ORR experiments were executed by firstly bubbling the electrolyte solution (0.1 M KOH) with high purity O_2 for 20 min, and then blanketing the solution with an O_2 atmosphere during the entire experiment. The linear sweep voltammogram (LSV) plots were recorded from -0.8 to 0.2 V (*vs*. Ag/AgCl) under different electrode rotating rates with the scan rate of 5 mV/s. All the LSV plots were recorded as measured that without IR correction. The number of transferred electrons (*n*) during the ORR process was firstly calculated according to the following Koutecky-Levich (K-L) equation:

$$\frac{1}{J} = \frac{1}{J_k} + \frac{1}{J_L} = \frac{1}{J_k} + \frac{1}{B\omega^{0.5}} \quad (1)$$

$$B = 0.62nF(D_{O_2})^{2/3}v^{-1/6}C_{O_2} \quad (2)$$

In the equation (1), the J is the measured current density, J_k is the kinetic current density, and ω is the rotating rate of the electrode. As for the equation (2), the n represents the number of transferred electrons during the ORR process, F is the Faraday constant (96500 C mol^{-1}), D_{O_2} is the diffusion coefficient of O_2 in the electrolyte (1.9×10^{-5} cm^2 s^{-1}), v is the kinetic viscosity (0.01 cm^2 s^{-1}), and C_{O_2} is the saturated concentration of O_2 (1.2×10^{-6} mol cm^{-3}).

Moreover, the n value and the yield of formed intermediate peroxide (HO_2^-) species were further calculated according to the RRDE method *via* the following equations:

$$n = 4\ I_d / (I_d + I_r/N) \quad (3)$$

$$HO_2^-\% = 200\ (I_r/N)/(I_d + I_r/N) \quad (4)$$

Where the I_d represents the disk current, I_r stands for the ring current, and N is the collection efficiency of the RRDE apparatus. Here, the N value is 0.37, as determined from the redox system that contains Fe^{II}/Fe^{III} ions.

For comparison, all potential values used in this study were normalized to that of the reversible hydrogen electrode (RHE) based on the formula: E (RHE) = E (Ag/AgCl) + 0.197 + 0.0591*pH.

Poisoning or blocking single-atom sites experiments: It is known that SCN^- ions can poison M-N_x active sites during catalysis of ORR. To consider the potential reaction between SCN^- ions and KOH,

the ORR activity of Cu,Co-N-C NSs was further measured in O_2-saturated 0.1 M $HClO_4$ containing 0.01 M NaSCN, and compared with that examined in pure 0.1 M $HClO_4$ solution.

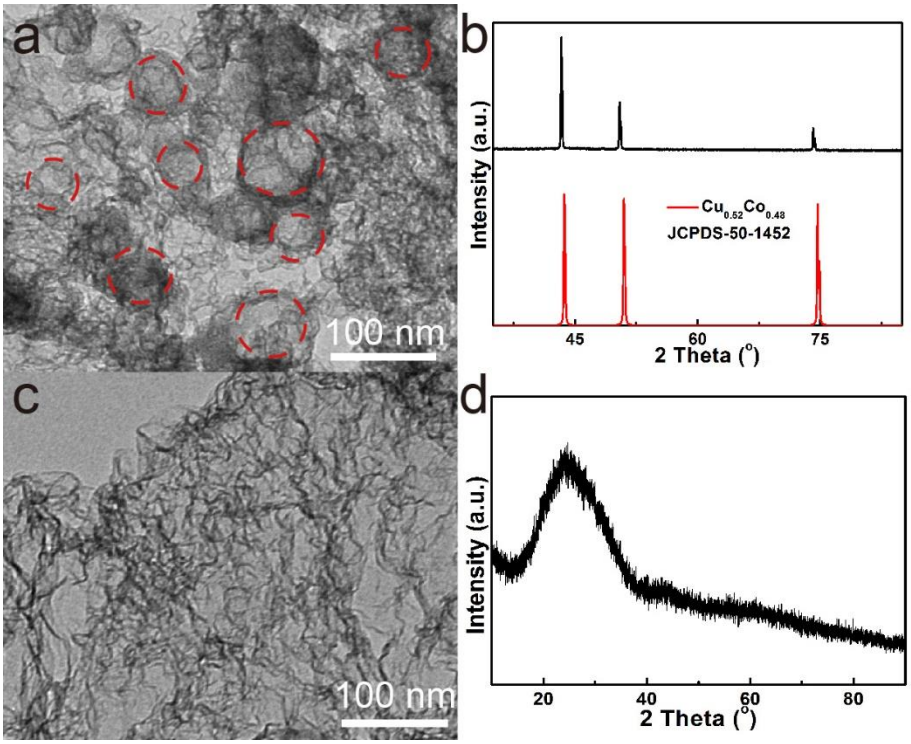

Fig. S1 (a-b) TEM image and XRD pattern of the CuCo/Cu,Co-N-C intermediates. (c-d) TEM image and XRD pattern of the CuCo/Cu,Co-N-C intermediates after acid etching.

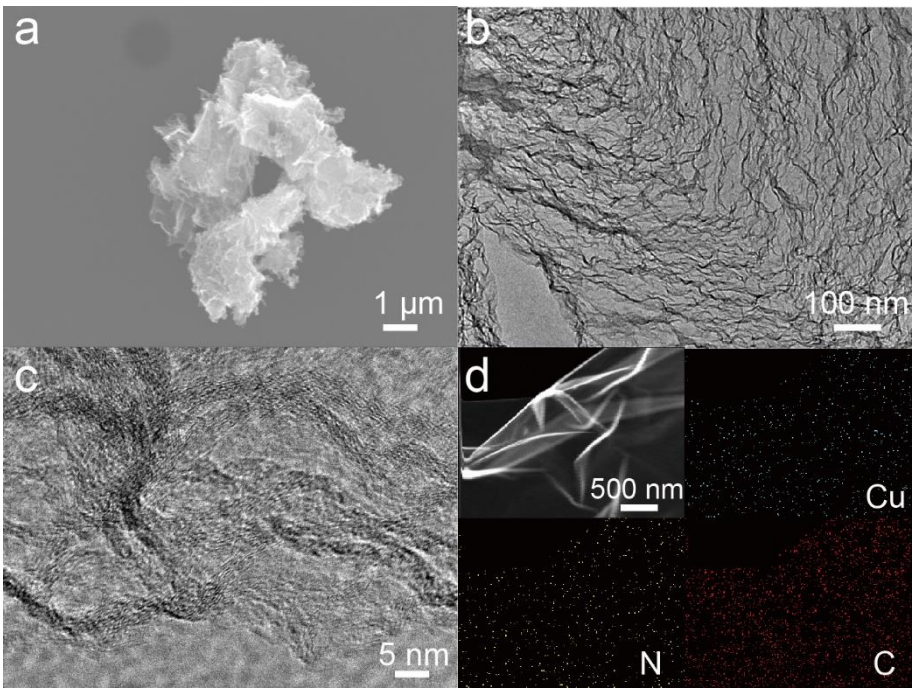

Fig. S2 (a) FE-SEM image of Cu-N-C. (b-c) TEM and HRTEM images of Cu-N-C. (d) Corresponding low magnification HAADF-STEM image and elemental mapping analyses for Cu-N-C.

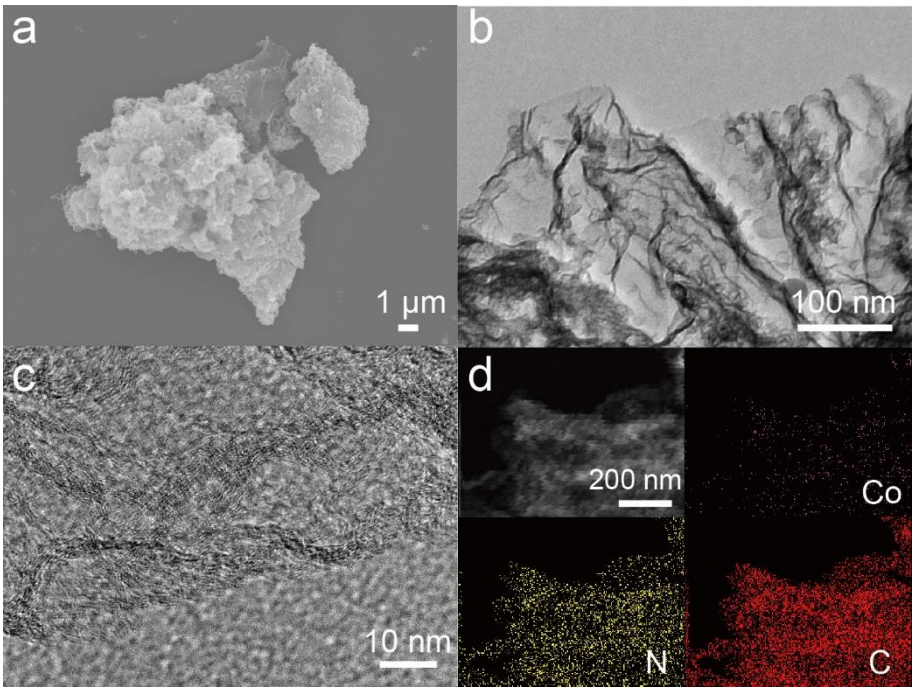

Fig. S3 (a) FE-SEM image of Co-N-C. (b-c) TEM and HRTEM images of Co-N-C. (d) Corresponding low-magnification HAADF-STEM image and elemental mapping analyses for Co-N-C.

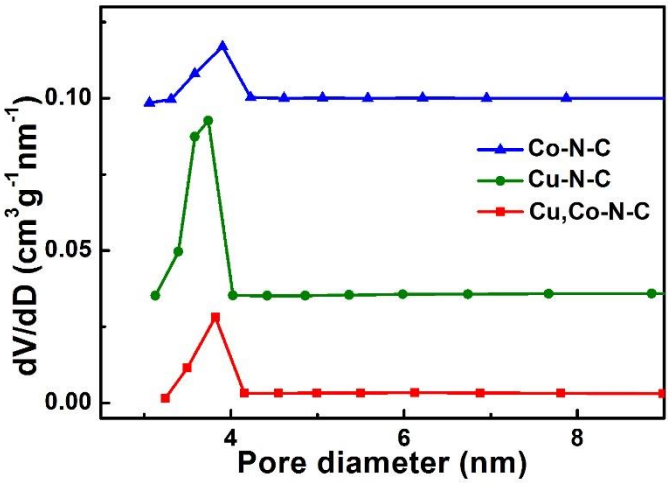

Fig. S4 The pore-size distribution plots for Cu,Co-N-C NSs (red plot), Cu-N-C (green plot) and Co-N-C (blue plot) samples.

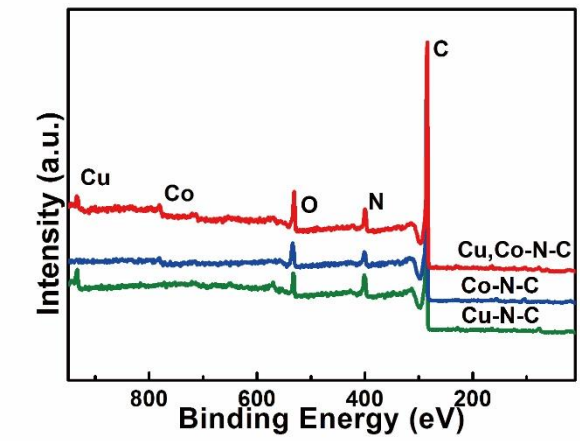

Fig. S5 The survey XPS spectra for Cu,Co-N-C NSs (red plot), Cu-N-C (green plot) and Co-N-C (blue plot) samples.

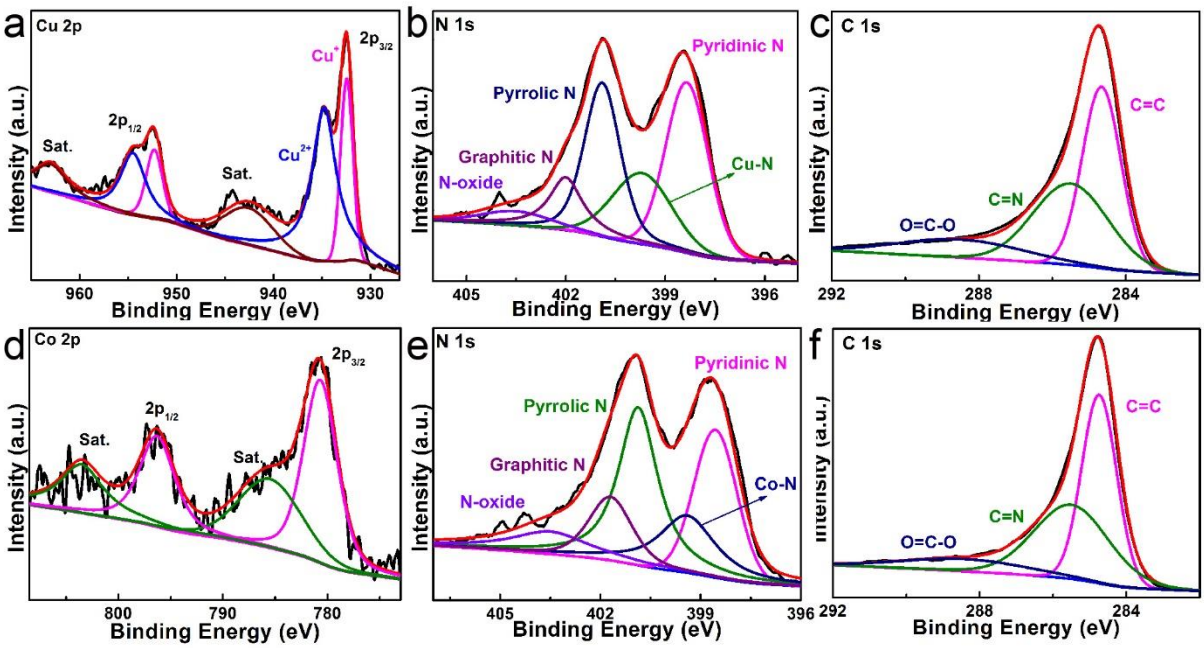

Fig. S6 (a-c) Core-level XPS spectra for Cu 2p (a), N 1s (b), and C 1s (c) peaks of Cu-N-C NSs. (d-f) Core-level XPS spectra for Co 2p (d), N 1s (e), and C 1s (f) peaks of Co-N-C NSs.

Table S1. Comparing the content of various nitrogen species in Cu,Co-N-C NSs, Cu-N-C, and Co-N-C samples based on XPS data

Sample	Species percentage (%)				
	Pyridinic N	Metal-N_X	Pyrrolic N	Graphitic N	Oxidized N
Cu,Co-N-C	35.8	19.4	15.5	20.7	8.5
Cu-N-C	33.6	20.0	29.2	12.0	5.2
Co-N-C	24.6	17.9	34.4	12.8	10.3

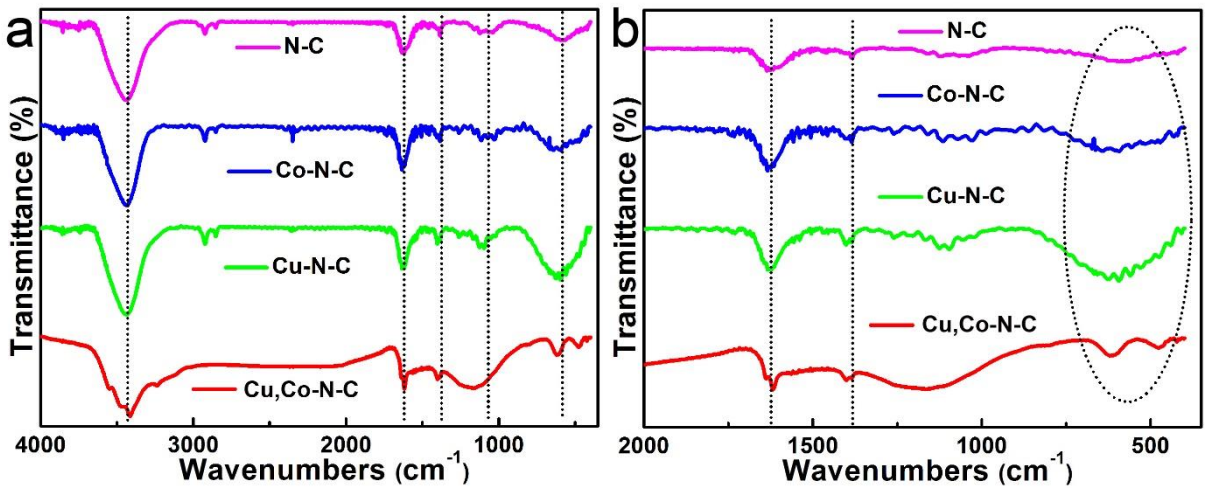

Fig. S7 (a) FT-IR spectra for Cu,Co-N-C NSs, pure Cu-N-C, Co-N-C, and N-C samples at 4000 to 400 cm^{-1}. (b) The magnified FT-IR spectra for Cu,Co-N-C NSs, pure Cu-N-C, Co-N-C, and N-C samples at 2000 to 400 cm^{-1} region.

Discussion and Analysis of FT-IR spectra:

The above **Fig. S7** shows the FT-IR spectra for Cu,Co-N-C NSs, pure Cu-N-C, Co-N-C and N-C samples. As for pure N-C sample, it shows four main characteristic absorption bands at 3436 cm^{-1}, 1622 cm^{-1}, 1386 cm^{-1}, and 581 cm^{-1}, which can be assigned to the -NH stretching vibration, -C=C or -C=N stretching vibration from the skeleton of graphitized carbon structures, -C-N stretching vibration, and the in-plane bending or deformation vibration of N-containing heterocycles (*e.g.* pyrrolic ring), respectively(*The Infrared Spectra of Complex Molecules*, L. J. Bellamy, Ed., Chapman and Hall, Ltd. London, **1975**; *ACS Nano* **2019**, *13*, 3177). While for pure Cu-N-C and Co-N-C, the featured absorption bands for -C=C/-C=N stretching vibration, -C-N stretching vibration and N-heterocycles in-plane bending or deformation vibration, are shifted to high wavenumber direction about 10~18 cm^{-1}, indicating that the Cu or Co has been incorporated into the N-C matrix, and bonded with the N to form Cu-N_x or Co-N_x coordination geometry. Usually, the absorption band at the low wavenumber region (400-1000 cm^{-1}) is served as the indicator for the formation of metal-N coordination (*J. Phys. Chem.* **1956**, *60*, 934). Both the Cu-N-C and Co-N-C only exhibit a broad absorption band centered at about 599 cm^{-1}, implying that their metal-N coordination mode or environment may be similar. Whereas for Cu,Co-N-C sample, it shows two obvious absorption bands at 476 and 617 cm^{-1} in the

low wavenumber region, implying that the introducing of Cu and Co bimetal will vary the metal-N coordination mode or environment, unlike their mono-metallic counterparts. The presence of those two peaks for metal-N coordination in Cu,Co-N-C NSs gives a hint that the following two kinds of metal-N coordination modes may exist in this sample: (1) the presence of isolated Cu-N_x and Co-N_x coordination centers; (2) the occurrence of "married" N_x-Cu-Co-N_x or (Cu,Co)-N_x bimetallic coordination sites with the bonding between Cu and Co atomic centers, similar to previously reported (Fe,Co)/N-C dual site catalyst (*J. Am. Chem. Soc*. **2017**, 139, 10976). If the first case actually occurs in our Cu,Co-N-C sample, its Cu 2p and Co 2p fine XPS spectra should be identical to that of Cu-N-C and Co-N-C, respectively, and no charge transfer between Cu and Co could be observed. By carefully comparing the Cu 2p and Co 2p fine XPS spectra of Cu,Co-N-C with those of Cu-N-C and Co-N-C, the obvious charge transfer has been observed in Cu,Co-N-C sample (please see Fig. 4a and Fig. 4b). Thus, the first case can be excluded. And the most possible situation is that the Cu,Co-N-C sample mainly adopts the second metal-N coordination mode, *i.e*., the formation of N_x-Cu-Co-N_x or (Cu,Co)-N_x bimetallic sites.

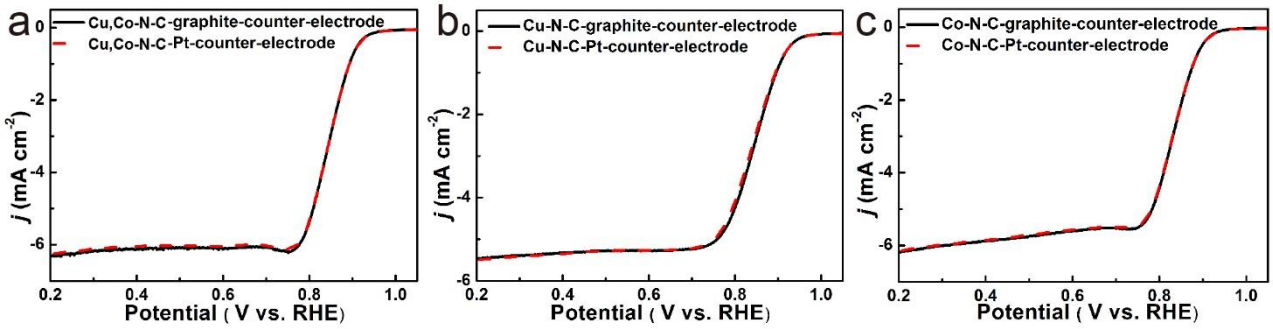

Fig. S8 (a) Comparing the LSV curves of bimetal Cu,Co-N-C NSs catalyst that measured at 1600 rpm by using high-purity graphite rod and Pt foil as the counter-electrode, respectively. (b) Comparing the LSV curves of pure Cu-N-C control catalyst that measured at 1600 rpm by using high-purity graphite rod and Pt foil as the counter-electrode, respectively. (c) Comparing the LSV curves of pure Co-N-C control catalyst that measured at 1600 rpm by using high-purity graphite rod and Pt foil as the counter-electrode, respectively.

Table S2. Comparing the ORR performance parameters of Cu,Co-N-C NSs with other reported M-N-C catalysts (in 0.1 M KOH electrolyte)

Catalyst	Doped element	Onset potential (V vs. RHE)	Half-wave potential (V vs. RHE)	References
Cu,Co-N-C NSs	Cu, Co, N	0.93	0.85	This work
Nano-P-ZIF-67	Co, N	1.01	0.899	*J. Power Sources* 2017, *368*, 46-56
HNCSs	Zn, N	0.92	0.82	*Carbon* 2019, *146*, 248-256
Cu-N-C NDs	Cu, N	0.97	0.85	*Small* 2019, *15*, 1902410
Fe_xN/NC-7	Fe, N	0.98	0.885	*Appl. Catal., B* 2020, *268*, 118405
Fe/Co-NCs	Fe, Co, N	0.963	0.877	*Carbon* 2019, *146*, 671-679
Fe-N-C	Fe, N	0.96	0.83	*J. Power Sources* 2018, *375*, 214-221
Co@Co-N-C-ANHs	Co, N	0.98	0.85	*Appl. Catal., B* 2020, *260*, 118207
Co-N-C	Co, N	0.98	0.889	*J. Power Sources* 2019, *418*, 50-60
Fe-SAs/Fe_3C-Fe@NC	Fe, N	0.98	0.927	*Small* 2020, *16*,1906057
3DOM Fe-N-C-900	Fe, N	0.92	0.875	*Nano Energy* 2020, *71*, 104547
Fe-N-C/MXene	Fe, N	0.92	0.84	*ACS Nano* 2020, *14*, 2436-2444
Fe(0)@FeNC	Fe, N	0.946	0.852	*Appl. Catal., B* 2019, *251*, 240-246
Fe-N-C SA/HCF	Fe, N	0.931	0.802	*Small* 2020, *16*, 1905920
Sc@NG	Sc, N	0.99	0.89	*J. Power Sources*, 2019, *431*, 265-273
(Fe,Co)/CNT	Fe, Co, N	1.15	0.954	*Energy Environ. Sci.*, 2018,*11*, 3375-3379

3D Co@N/C	Co, N	0.915	0.812	*Carbon* 2019, *153*, 575-584
NC/$Fe_{10-x}Co_x$	Fe, Co, N	0.97	0.87	*J. Alloys Compd.* 2017, *710*, 57-65

[**Notes**]: The abbreviations of "NSs", "ZIF", "HNCSs", "NDs", "NHs", "NC", "3DOM", "SA/HCF", "NG" and "CNT" in the listed catalysts represent the "nanosheets", "zeolite imidazole framework", "hollow N-doped carbon microspheres", "nanodisks", "nanohybrids", "nanoarchitectures", "3D hierarchically ordered microporous-mesoporous-macroporous", "single atoms in hyphae-derived carbon fibers", "N-doped graphene" and "carbon nanotubes", respectively. While for the symbol of "@", it stands for the "core-shell nanostructures".

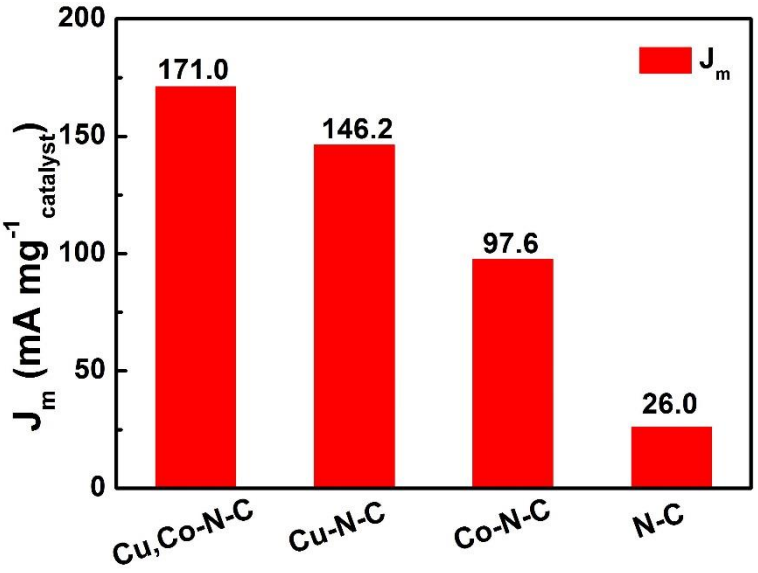

Fig. S9 Comparing the mass activities (J_m) of the typical Cu,Co-N-C NSs, pure Cu-N-C, pure Co-N-C and N-C catalysts at 0.80 V (*vs*. RHE).

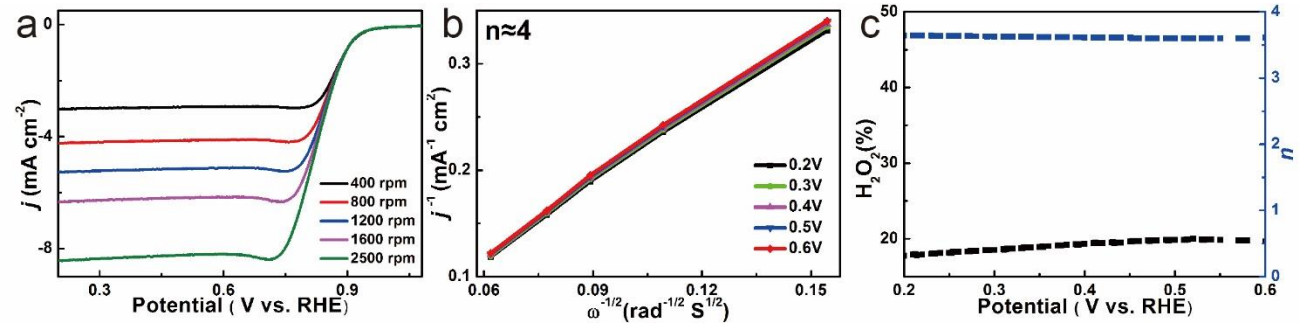

Fig. S10 (a) ORR polarization curves of Cu,Co-N-C NSs that measured in 0.1 M KOH electrolyte at the electrode rotating rate ranging from 400 to 2500 rpm. (b) Corresponding K-L plots at various potentials. (c) The yield of peroxide species and the number of transferred electrons (n) at different potentials for Cu,Co-N-C NSs that obtained by RRDE tests.

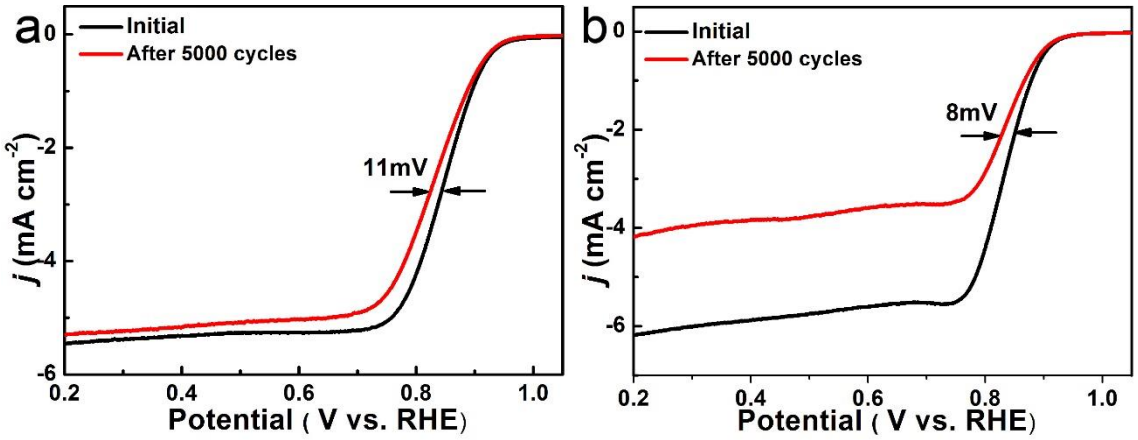

Fig. S11 (a) Durability tests of Cu-N-C control catalyst in O_2-saturated 0.1 M KOH for continuously working 5000 cycles (30h). (b) Durability tests of Co-N-C control catalyst in O_2-saturated 0.1 M KOH for continuously working 5000 cycles (30h).

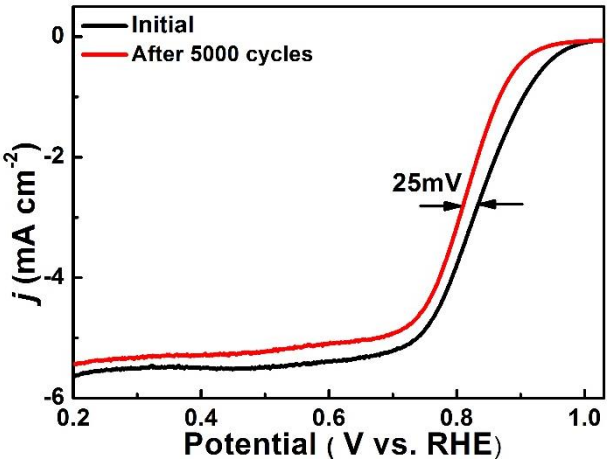

Fig. S12 Durability test for commercial Pt/C (20%) catalyst in O_2-saturated 0.1 M KOH electrolyte.

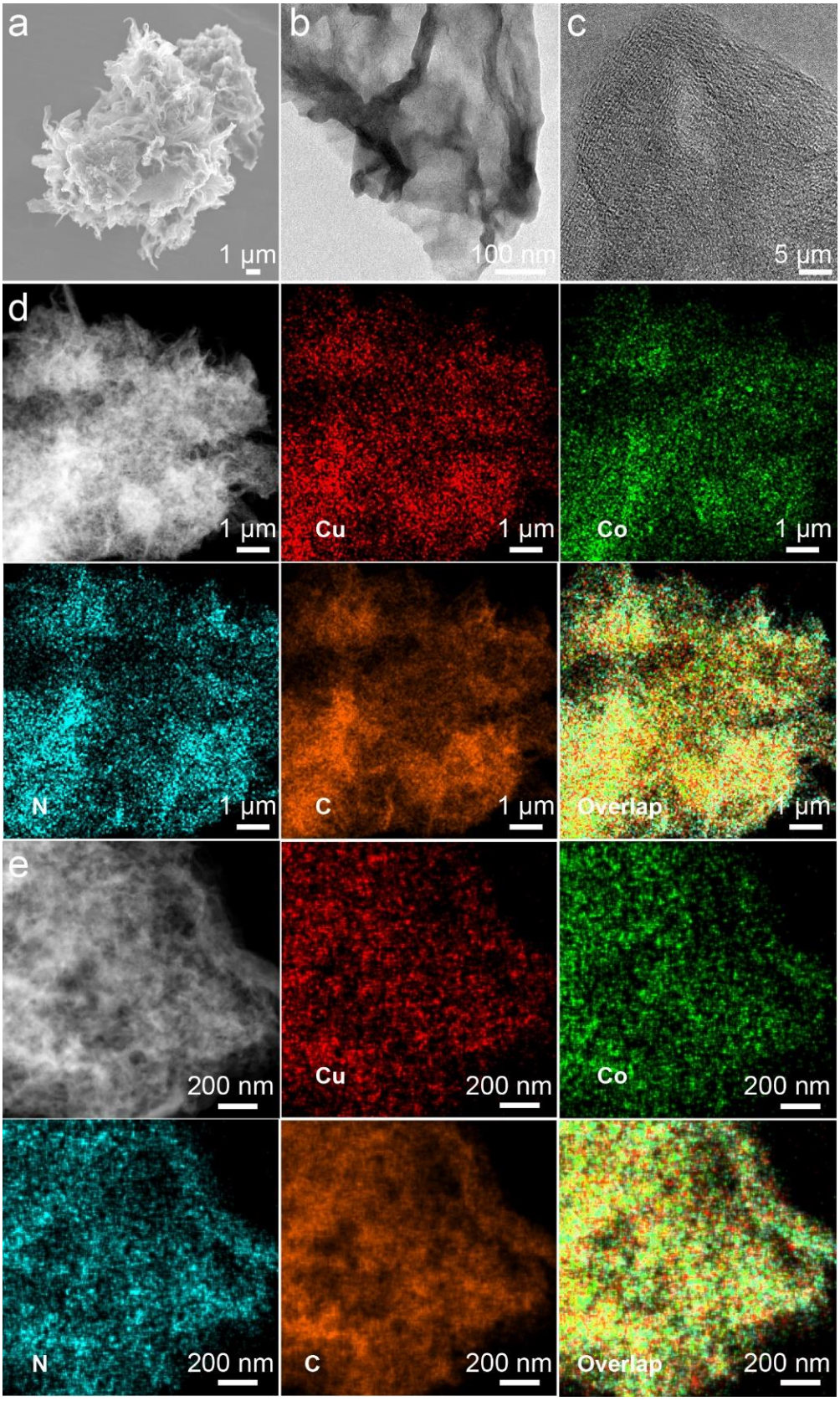

Fig. S13 (a) FE-SEM image of Cu,Co-N-C NSs sample that collected after ORR tests for 5000 cycles. (b-c) The corresponding TEM (b) and HRTEM (c) images for Cu,Co-N-C NSs sample after ORR

cycling tests. (d) Low-magnification HAADF-STEM image and elemental mapping analyses for Cu,Co-N-C NSs sample after ORR cycling tests. (e) The related high-magnification HAADF-STEM image and elemental mapping analyses for Cu,Co-N-C NSs after ORR cycling tests.

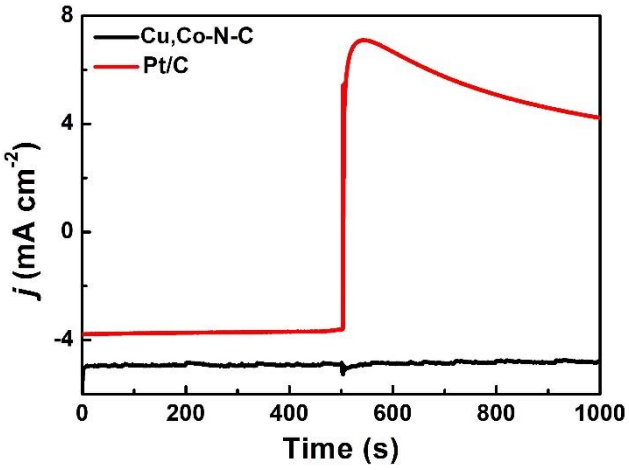

Fig. S14 Chronoamperometric response of Cu,Co-N-C NSs and Pt/C catalyst at 0.30 V (*vs*. RHE) by adding 1M methanol into O_2-saturated 0.1 M KOH electrolyte after 500 s.

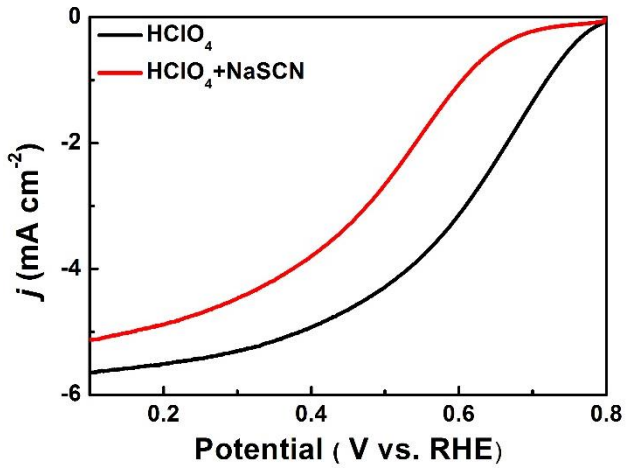

Fig. S15 ORR polarization curves of Cu,Co-N-C NSs in O_2-saturated 0.1 M $HClO_4$ electrolyte with or without adding 0.01 M NaSCN.